# Identification and Computation of Individual Propeller Acoustics of the Joby Aviation Aircraft

Austin D. Thai* and Jeremy J. Bain†
*Joby Aviation, Santa Cruz, CA*

Kyle A. Pascioni‡
*NASA Langley Research Center, Hampton, VA*

**The individual propeller sources of the Joby Aviation aircraft are separated using an order tracking filter on measurement data and computed using high-fidelity computational fluid dynamics (CFD) to quantify the relative contributions to the total noise. Computational results are verified against experimental data for hover and steady level flight at 60 knots and demonstrate very good agreement of both overall sound pressure level magnitude and directivity. The propeller source separation for hover shows good agreement between the methods except for the inboard propellers, and it is expected that the assumptions in the CFD model do not accurately capture the flight test condition. Both methods are able to separate the higher tonal levels generated by the tail propellers due to the aerodynamic interaction. Overall, considering the discrepancies between the CFD model and flight test, the agreement in Vold-Kalman-filtered results and prediction yields confidence that the separation method is successful.**

## I. Nomenclature

| | | |
|---|---|---|
| $L$ | = | Unweighted integrated sound pressure level [dB re. 20 $\mu$Pa] |
| $k$ | = | Shaft order |
| $s$ | = | Shaft index or propeller number |
| $t$ | = | Time [s] |
| $(x, y, z)$ | = | Local coordinate system for microphone measurement field [ft] |
| $\theta$ | = | Azimuth angle [deg] |
| $\phi$ | = | Elevation angle [deg] |

## II. Introduction

The advancement of electric vertical takeoff and landing (eVTOL) technology has encouraged research into understanding the aeroacoustics characteristics of such vehicles. Although preliminary findings have shown they are quieter than traditional vertical takeoff and landing (VTOL) aircraft [1, 2], there is still uncertainty as to their true acoustic sources. Higher solidity, lower tip Mach number eVTOL propellers can result in less prominent tonal noise peaks relative to the broadband levels. Distributed electric propulsion has enabled the usage of multiple thrusters, which may have mixed, varying rotation rates, further complicating the problem of source identification. Methods that are able to distinguish the noise sources of eVTOL aircraft will help provide insight into the physics of noise generation. In addition, identification of component contribution to the total acoustic signal can be used to validate computational tools. These tools may then be improved and, in turn, aid the design process, which benefits the next generation of aircraft.

*Acoustics Senior Engineer, Flight Physics. austin.thai@jobyaviation.com
†CFD and Aeroacoustics Lead, Flight Physics.
‡Research Aerospace Engineer, Aeroacoustics Branch.


**Fig. 1 The Joby Aviation pre-production prototype [Source: Joby Aviation].**

Stephens and Vold used the Vold-Kalman (V-K) filter to perform order tracking to separate the harmonic content of an open rotor [3]. The V-K filter method is advantageous over other filtering methods because it is able to extract time-varying amplitude and phase information from the original signal [4]. This method was first applied to flyover noise from rotorcraft by Rachaprolu and Greenwood, who were able to separate main rotor and tail rotor noise from a Bell 430 helicopter [5]. However, the rotation rates of a turbine-engine helicopter's rotors are relatively constant in flight when compared to those of an eVTOL aircraft. In addition, the rotation rates of an eVTOL aircraft's propellers will potentially be much closer in magnitude than those of the main rotor and tail rotor of a helicopter. It is still uncertain whether the acoustic signals of propellers with very similar rotation rates can be separated using the V-K filter.

In this study, the V-K filter method is used on flight test measurements to quantify the individual propeller contributions to the total acoustic levels of the Joby Aviation aircraft at two flight conditions, hover and steady level flight at 60 knots. High-fidelity computational fluid dynamics (CFD) simulations of the Joby aircraft are conducted for comparison of the magnitude and directivity of the V-K filter results. Thai et al. [6] presented NASA OVERFLOW computations of the Joby aircraft in steady level flight at 60 knots and 100 knots. Roget et al. [7] presented HELIOS computations using both mStrand and ROAM. Although they were able to highlight the significance of airframe noise, they did not separate the individual propeller components. In this work, an application of the V-K filter to ground-based acoustic measurements yields insight into the utility of the method for eVTOL aircraft. The separated noise levels and directivity help to characterize the individual propeller acoustics of the Joby aircraft in various flight regimes.

## III. Methods

### A. Experimental measurements

Joby Aviation partnered with the National Aeronautics and Space Administration (NASA) to conduct acoustic flight tests of the Joby aircraft in 2021 as part of the NASA Advanced Air Mobility National Campaign. The Joby aircraft, designed to carry one pilot and four passengers, has six tilting propellers, which enable transition from thrustborne to wingborne flight to achieve speeds up to 200 mph. The pre-production prototype is depicted in semi-thrustborne flight in Fig. 1. The shaft index, $s$, of each propeller is labeled in Fig. 2. The wingtip propellers correspond to $s = 1, 4$, the inboard propellers correspond to $s = 2, 3$, and the tail propellers correspond to $s = 5, 6$. The experimental campaign consisted of hover, both in and out of ground effect, steady level flight at various airspeeds, and several approach and departure trajectories. Over fifty groundboard microphones were set up to capture the noise levels. The vehicle flight states, including

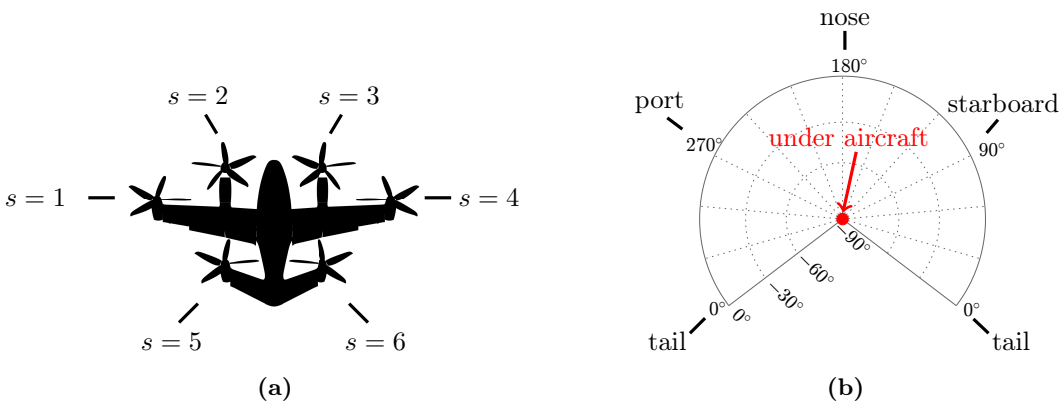


**Fig. 2 Diagrams indicating (a) the numbering scheme of $s$, the shaft index or propeller number, on the Joby Aviation aircraft and (b) the coordinate system of the acoustic hemisphere.**

aircraft position, propeller states, and flight controls, were recorded for data analysis. Pascioni et al. [8] presented some of the results at the 28th AIAA/CEAS Aeroacoustics Conference, providing insight into the acoustic characteristics of different flight regimes.

This paper will present further analysis of flights conducted as part of the acoustic flight test campaign. One hover-out-of-ground effect and one steady level flyover at 60 knots were chosen for investigation. For both flights, the average wind speed was less than 3 knots, which was favorable for acoustic measurements. For each microphone, the groundboard was assumed to be acoustically hard and a pressure de-doubling correction was applied. The signal was split into 0.5 second intervals, each of which were divided into 3 overlapping blocks. For each block, a Hamming window was applied before computing the Fourier transform and subsequent power spectrum. The power spectra calculated from the three blocks were averaged to obtain a spectrum for the entire interval. For the steady level flyover, a linear array of microphones was used to generate acoustic hemispheres to depict the aircraft directivity. The hemispheres depicted in this paper are rendered using a Lambert projection, as seen in Fig. 2b. The elevation angle $\phi$ runs from 0 deg on the horizon to -90 deg under the aircraft. The azimuth angle $\theta$ spans 360 degrees, with the nose of the aircraft at 180 deg, the tail at 0 deg, port at 270 deg, and starboard at 90 deg. The hemispheres were generated at a distance of 100 ft, greater than 10 times the propeller diameter.

### B. Propeller source separation

Proper implementation of the V-K filter method requires synchronizing the acoustic signals with the RPM measurements of each propeller. First, the acoustic pressure measurements from the experiments are halved to account for the pressure doubling caused by the groundboard. The signals are then de-Dopplerized and back-propagated to a distance of 100 ft from the aircraft. The measurements of the time-varying propeller rotation rates are upsampled to match the emission time calculated in the de-Dopplerization. Then, the second-generation multi-order V-K filter [9, 10] is applied to extract the time-varying amplitudes per shaft order, $k$, corresponding to each of the six individual propellers, representing shaft indices $s = 1 - 6$. The spectral levels are adjusted for atmospheric absorption based on the distance from each microphone location to a hemisphere at the corresponding emission angle, using the atmospheric condition measured during each flight. The mean standard deviation of RPM was approximately 44 RPM during the 60 knot flyover and 5 RPM for hover. The V-K filter model parameters used in this work were investigated by Pascioni et al. [11]. A single pole count and 1 Hz bandwidth were shown to improve accuracy and robustness of the source separation for the flight conditions in the current paper. It should be noted that the control system at the time of the flight test is not indicative of the control law intended for the production aircraft, and future work is needed to understand the limits of the utility of the V-K filter.

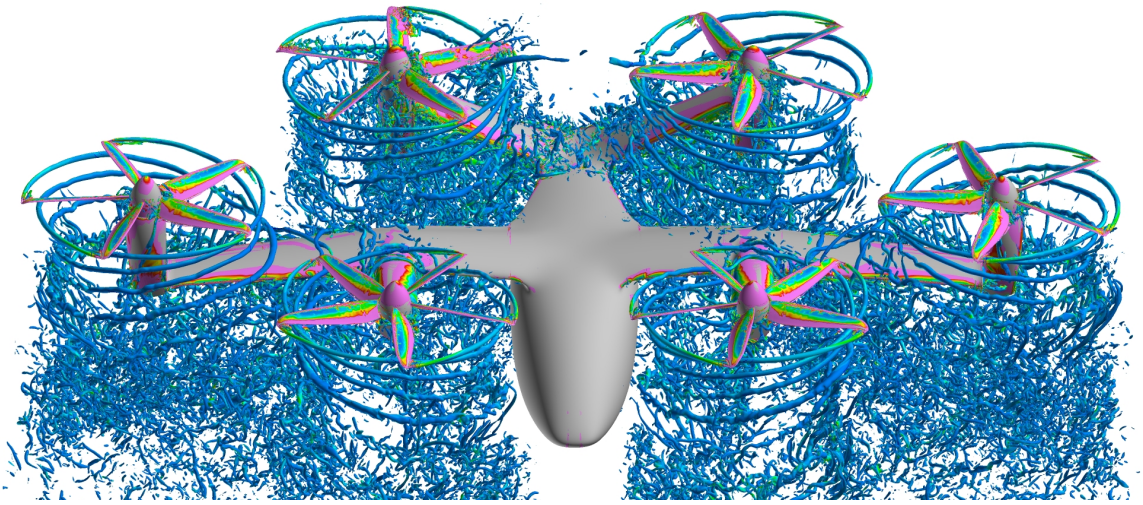

**Fig. 3 Flow visualization of the Joby aircraft in hover. Iso-surfaces of q-criterion are colored by vorticity magnitude.**

### C. Computational aeroacoustics

High-fidelity computational fluid dynamics (CFD) simulations of the Joby aircraft in hover and in steady level flight at 60 knots were conducted using the overset grid solver NASA OVERFLOW version 2.3e [12–14]. Delayed Detached Eddy Simulation (DDES) terms were used with the Spalart-Allmaras (SA) model for turbulence closure [15, 16]. Laminar-turbulent transition was predicted using the Amplification Factor Transport (AFT) model [17]. The simulation implemented the Harten-Lax-van Leer-Contact (HLLC) upwind scheme [18] and improved Successive Symmetric Overrelaxation (SSOR) algorithm [14] with 5th-order spatial differencing scheme and 2nd-order backward differencing. Both cases were conducted at a constant RPM that was equal across all propellers. However, the hover case modeled all six propellers while the 60 knots case modeled half the aircraft with a symmetry assumption. For both simulation cases, the propeller phasing was randomized to mitigate effects of wave interference, although these effects should be explored in the future. The aircraft was trimmed to lift using blade pitch in hover. For steady level flight at 60 knots, the aircraft was trimmed using blade pitch and aircraft angle of attack to lift, drag, and pitching moment. The simulations used a quarter degree time step and one revolution was extracted for acoustic post-processing.

The impermeable surface Farassat Formulation 1A implementation within PSU-WOPWOP [19] was used to compute the far-field acoustics with compact chordwise sources. At low speeds, the propeller contribution dominates and Thai et al. [20] demonstrated good agreement using this method for approach and departure noise. The propellers were simulated separately in PSU-WOPWOP so that their individual acoustic levels could be compared to V-K filter output. For hover, the observers were placed on the microphone field at their relative position to the aircraft and the individual propeller pressures were summed in the time domain to arrive at the total aircraft acoustic pressure signal. For the 60 knot flyover, the observers were placed on the 100 ft hemisphere. At this speed, the RPM variation is larger and so the total aircraft levels were obtained by summing the acoustic spectra incoherently to avoid the effects of constructive and destructive interference from propeller phasing. Other propagation effects, such as acoustic scattering and atmospheric attenuation, were not included in the model.

# IV. Hover

## A. Computational validation

In this section hover simulations are compared with experimental acoustic measurements of hover-out-of-ground effect. The hover simulations modeled the full airframe and six propellers in the OVERFLOW solver. The six propellers were simulated at a constant speed of 700 RPM, and the phase of each propeller was randomized at the beginning of the simulation. Flow visualization from the hover simulation, depicting iso-surfaces of q-criterion colored by vorticity magnitude, can be seen in Fig. 3. The flow solver is able to capture the generation of the tip vortices and their propagation into the wake. The relative propeller positioning and their placement with respect to the aircraft affect the aerodynamic interactions and thus the acoustic sources.

The experimental pressure data were recorded over a period of 12 seconds and halved to account for the effect of the groundboard. The 12 second period was split into 0.5 second segments to generate a spectral time history of the acoustic levels. A comparison of predicted and measured spectra for an observer at -19 deg elevation, 174 deg azimuth, near the nose of the aircraft, is plotted in Fig. 4. The solid black lines represent the bounds of the experimental range of measured spectra over the 12 second period, and the blue dashed line represents the mean value. The CFD-predicted spectrum, plotted in red, demonstrates very good agreement with the experimental data. The highest level is seen at the blade passage frequency (BPF) and agrees well with the mean level in the experiment. The CFD data cut off at the Nyquist frequency, but the levels are near-ambient at that end of the spectrum.

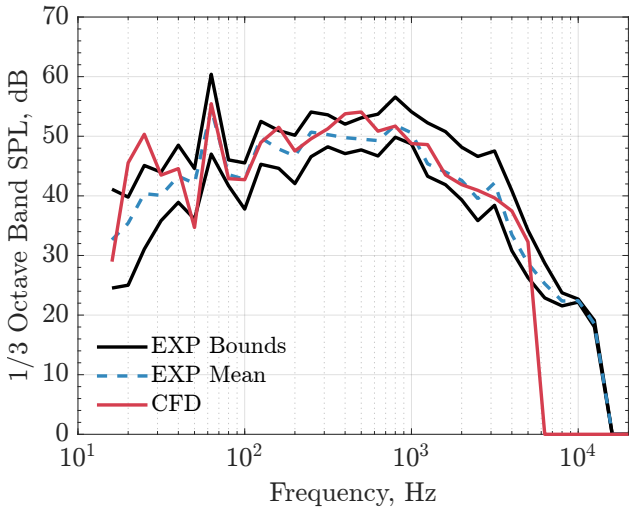


**Fig. 4 Comparison of predicted and measured one-third octave band sound pressure level in hover for an observer located at approximately -19 deg elevation and 174 deg azimuth, near the direction of the aircraft nose.**

The computed and measured hover ground contours of overall sound pressure level, $L$, are plotted in Fig. 5. The 3D coordinate system, $(x, y, z)$, was defined relative to a single microphone placed at the origin. The aircraft heading is approximately in the $-x$ direction. The experimental mean was computed over the 12 second period. The microphones are denoted by white circles and the projected aircraft ground location is marked as a black $\times$. The contour area of the highest level, located directly under the aircraft, is larger in the computations than in the experiments. In reality, the presence of the fuselage and the propeller downwash will affect the measurements and acoustic propagation. Overall, the magnitude and directivity show very good agreement. The overall sound pressure level difference computed relative to the total experimental range, $\Delta L$, is also shown in Fig. 5. The range of the experimental values is quite large due to the variability of the acoustic levels in hover, and the CFD prediction generally lies within the minimum and maximum measured $L$ for each microphone. Therefore, $\Delta L$ is zero for most of the measurement field and less than 2 dB everywhere.

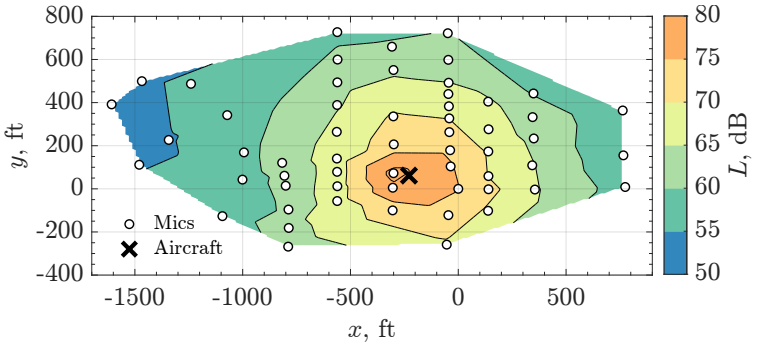


**(a) Experimental Mean**

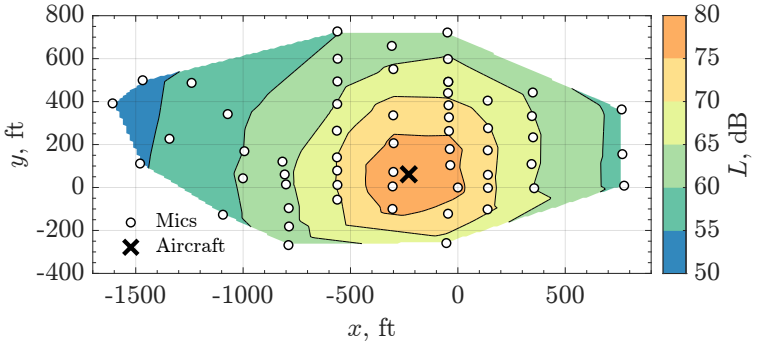


**(b) OVERFLOW + PSU-WOPWOP**

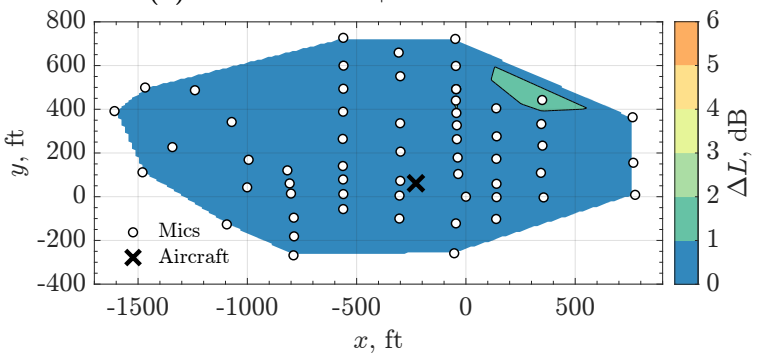


**(c) Difference Relative to Experimental Range**

**Fig. 5 Comparison between measured and predicted overall sound pressure level for the Joby aircraft in hover. The aircraft heading is approximately in the $-x$ direction. The difference is computed with respect to the range of measured values.**

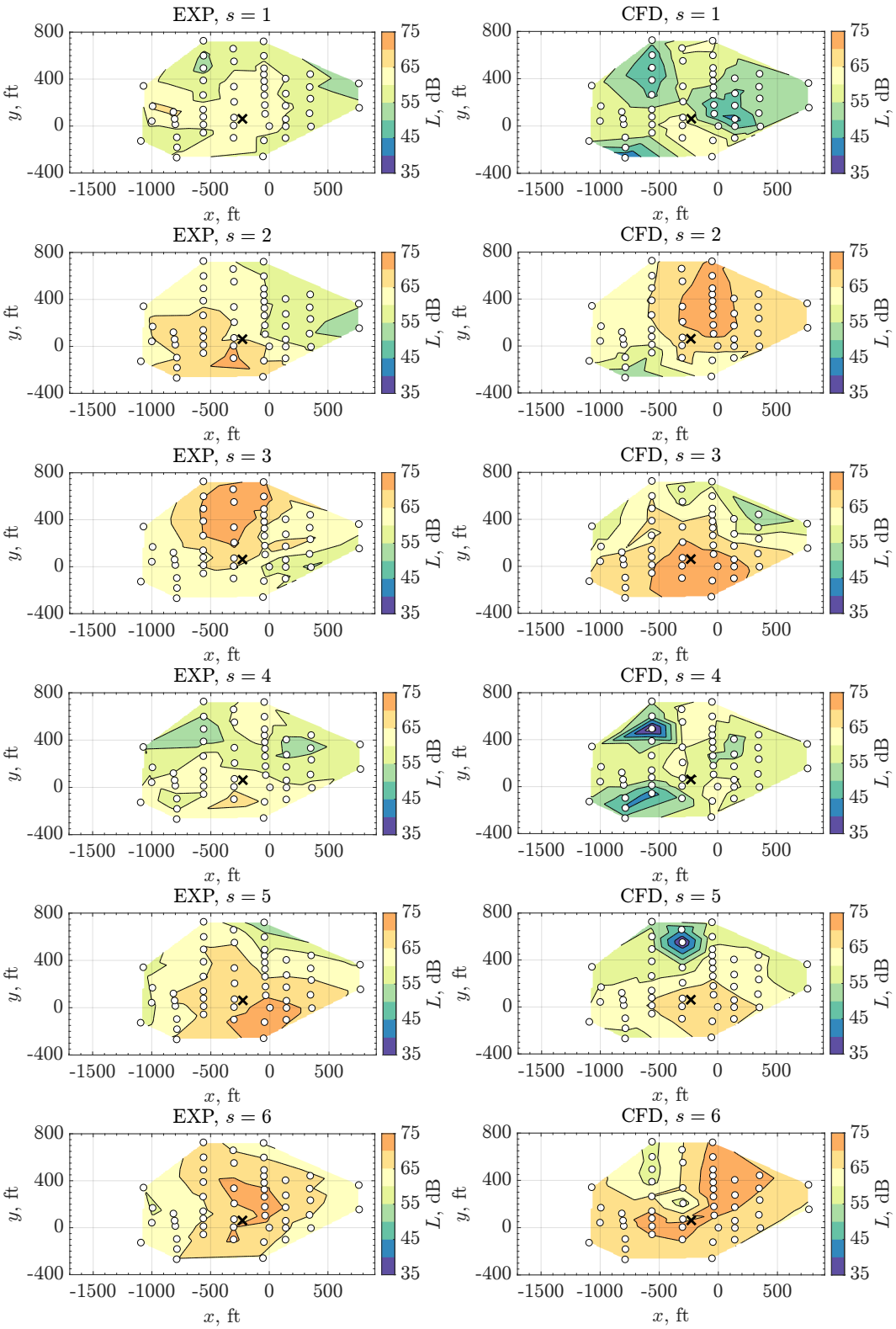


**Fig. 6 Comparison of experimental and OVERFLOW/PSU-WOPWOP predicted individual propeller BPF SPL for the Joby aircraft in hover. The levels have been adjusted using spherical spreading to a 100 ft distance. The circles mark the microphone locations and the $\times$ marks the aircraft position.**

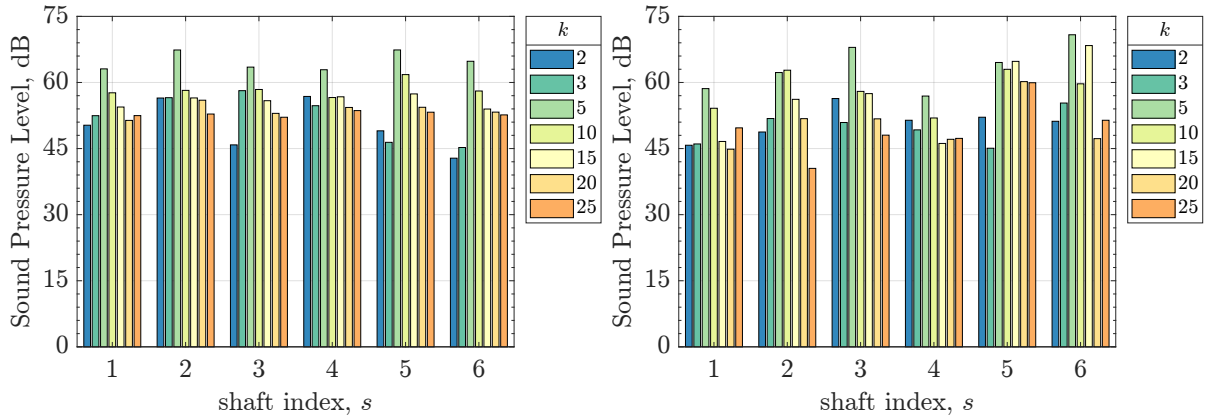


**(a) Experiment** **(b) CFD**

**Fig. 7 Comparison between mean V-K-filtered and predicted shaft sound pressure levels per order for the Joby aircraft in hover at a microphone near -36 deg elevation and 176 deg azimuth. The levels were adjusted to a distance of 100 ft assuming spherical spreading.**

### B. Propeller source separation

The V-K filter was applied to the hover-out-of-ground effect to separate the blade passage frequency ($k = 5$) contributions of the individual propellers. The individual propeller pressure signals from the hover simulations were computed separately for comparison. Contour maps of the BPF SPL over the microphone field are shown per propeller in Fig. 6. The levels have been back-propagated to a distance of 100 ft assuming spherical spreading to better highlight the directivity of the sources. Again, the microphones are denoted by white circles and the projected aircraft ground location is marked as a black $\times$.

There is reasonable agreement for the wingtip propellers ($s = 1, 4$). There are stronger cold spots of low levels in the CFD because the aircraft is simulated at a steady control state whereas the experiment has more variability. There is similarly good agreement for the tail propellers ($s = 5, 6$). The predicted levels are higher behind the aircraft and qualitatively match that of the experiment. However, there is poor agreement between the measured and predicted levels from the inboard propellers ($s = 2, 3$). While the peak levels across the field are similar, the predicted directivity seems to be opposite across the aircraft centerline when compared to the experiment. The V-K filter reveals higher levels for each inboard propeller on the same side of the aircraft, i.e., propeller 2 has stronger directivity on the port side. However, the CFD predicts higher levels on the opposite side, i.e., propeller 2 has stronger directivity on the starboard side. There are many other realistic effects that are not modeled, such as acoustic scattering from the airframe, wind, and atmospheric turbulence. Incorporation of additional physical phenomena could improve correlation.

The V-K filter was applied to obtain levels of other shaft orders ($k = 2 - 25$). The mean measured and predicted results for all propellers are plotted for a single microphone towards the nose of the aircraft, near -36 deg elevation and 176 deg azimuth, in Fig. 7. The levels were adjusted to a distance of 100 ft assuming spherical spreading for comparison. The measured levels have a trend across $s$, with the highest levels at the BPF. For this microphone near the aircraft centerline, one would expect similar levels among propeller pairs (inboard, wingtip, tail) due to the aircraft symmetry. This is generally true for the experiment. When comparing the propeller pairs, the mean difference in levels across all shaft orders is approximately 2.35 dB for the wingtip propellers, 2.95 dB for the inboard propellers, and 2.69 dB for the tail propellers. However, this is not the case for the CFD results, which yield different high frequency results for the inboard and tail propeller pairs. The mean difference in predicted levels across all shaft orders is approximately 2.55 dB for the wingtip propellers, 3.99 dB for the inboard propellers, and 6.50 dB for the tail propellers. It should be noted that the CFD is based on a single revolution with constant propeller phasing, and it is possible that introducing RPM variations, averaging runs with randomized phasing, or simply running more revolutions for acoustics could change the results.

To quantify the comparison across all microphones, the mean difference was computed and plotted per shaft order and index in Fig. 8. The difference was computed relative to the range of values over the measurement

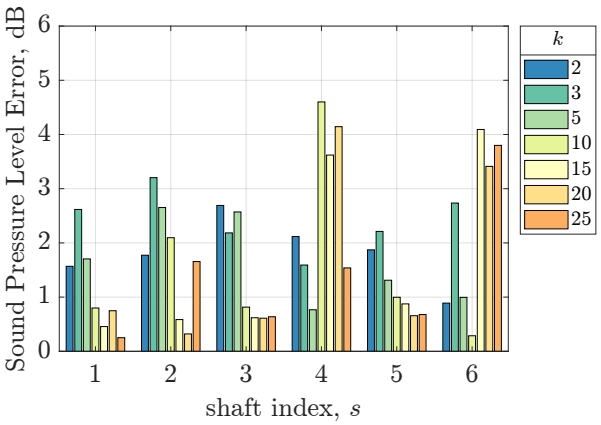


**Fig. 8 Mean difference between V-K-filtered and predicted shaft sound pressure levels per order in hover over all microphones. The difference was computed relative to the range of V-K-filtered values over the processing period.**

period and was less than 5 dB for all shaft orders and indices. There is a larger difference at the lower frequencies for most of the propellers except for propellers 4 and 6, where there is more significant discrepancy at the higher frequencies. It is still unknown as to the source of the differences between measurement and prediction. However, the mean difference across all microphones, orders, and indices was 1.75 dB, which gives confidence in the models.

## V. Steady Level Flight at 60 knots

### A. Computational validation

CFD simulations of the Joby aircraft in steady level flight at 60 knots were conducted and compared to flight test acoustic measurements. The CFD simulations were conducted as half aircraft with a symmetry assumption. The propellers were simulated at an equal constant 650 RPM at 47 deg tilt. A rendering of the flow visualization can be seen in Fig. 9. The simulation is able to capture the stronger tip vortices on the advancing side of the propeller disk. In this condition, there is aerodynamic interaction between the front propellers and the tail propellers, which is thought to affect performance and noise.

The predicted overall sound pressure level, $L$, was computed by adding the frequency spectra of the individual propellers incoherently to avoid the effects of constructive and destructive interference. A comparison of the predicted and measured $L$ on the 100 ft hemisphere is shown in Fig. 10. Although the experimental measurement does not cover the entire hemisphere, there is excellent agreement in peak levels, which were below 84 dB. There is also a good agreement in the directivity, with higher levels below the aircraft and lower levels forward. There is an overprediction on the sidelines and in front of the aircraft, which could indicate some modeling deficiency. Previous work that explored airframe acoustic scattering for this exact condition revealed a potential for acoustic shielding to have an impact in these regions of the directivity [6]. Nonetheless, the CFD is capturing the overall levels quite well considering the assumptions in the model.

### B. Propeller source separation

The V-K filter was applied to steady level flight at 60 knots. This condition is more challenging to filter than hover because it requires incorporating the varying aircraft position into the time synchronization of the propeller rotation rate with the acoustic pressure signal. The propeller levels were computed on the 100 ft hemisphere based on a single line of microphones from a single run. The extracted blade passage frequency, $k = 5$, sound pressure level across all propellers was plotted against the CFD in Fig. 11. The directivity is qualitatively similar to that of the overall sound pressure level, since the BPF dominates the spectrum in this condition. There is good agreement in the directivity and magnitude, except for in front of the aircraft where the CFD predicts higher levels.

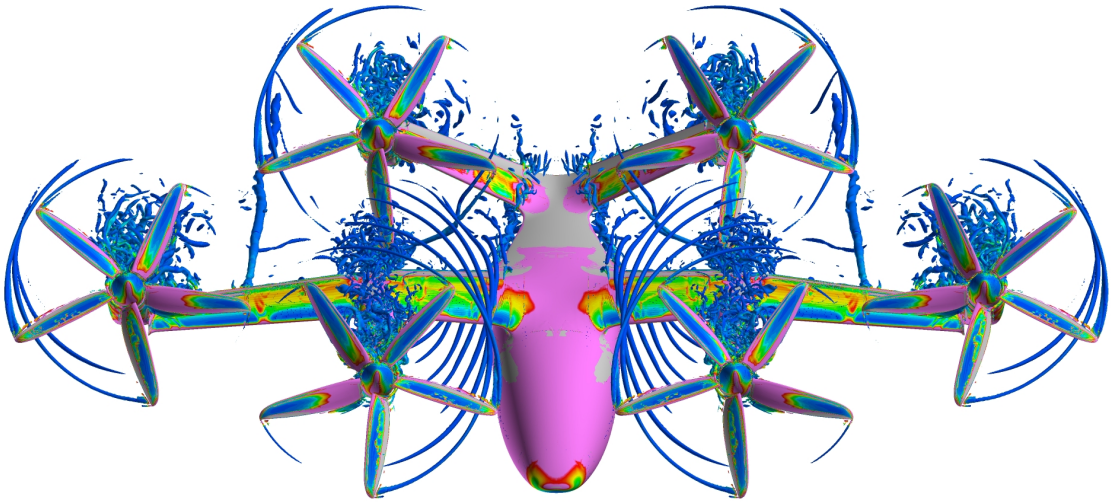

**Fig. 9 Flow visualization of the Joby aircraft in steady level flight at 60 knots. Iso-surfaces of q-criterion are colored by vorticity magnitude.**

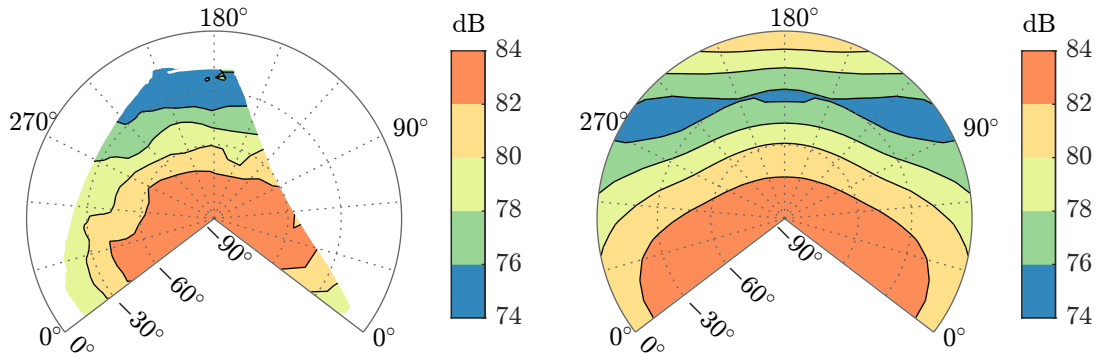


**(a) Experiment** **(b) CFD**

**Fig. 10 Comparison between measured and predicted overall sound pressure level for the Joby aircraft at 60 knots on a 100 ft hemisphere.**

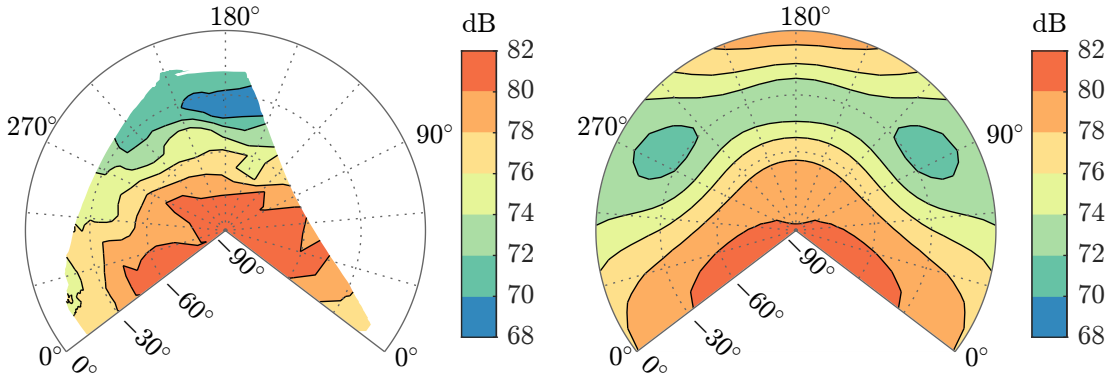


**(a) Experiment** **(b) CFD**

**Fig. 11 Comparison between V-K-filtered and predicted blade passage frequency sound pressure levels for the Joby aircraft at 60 knots on a 100 ft hemisphere.**

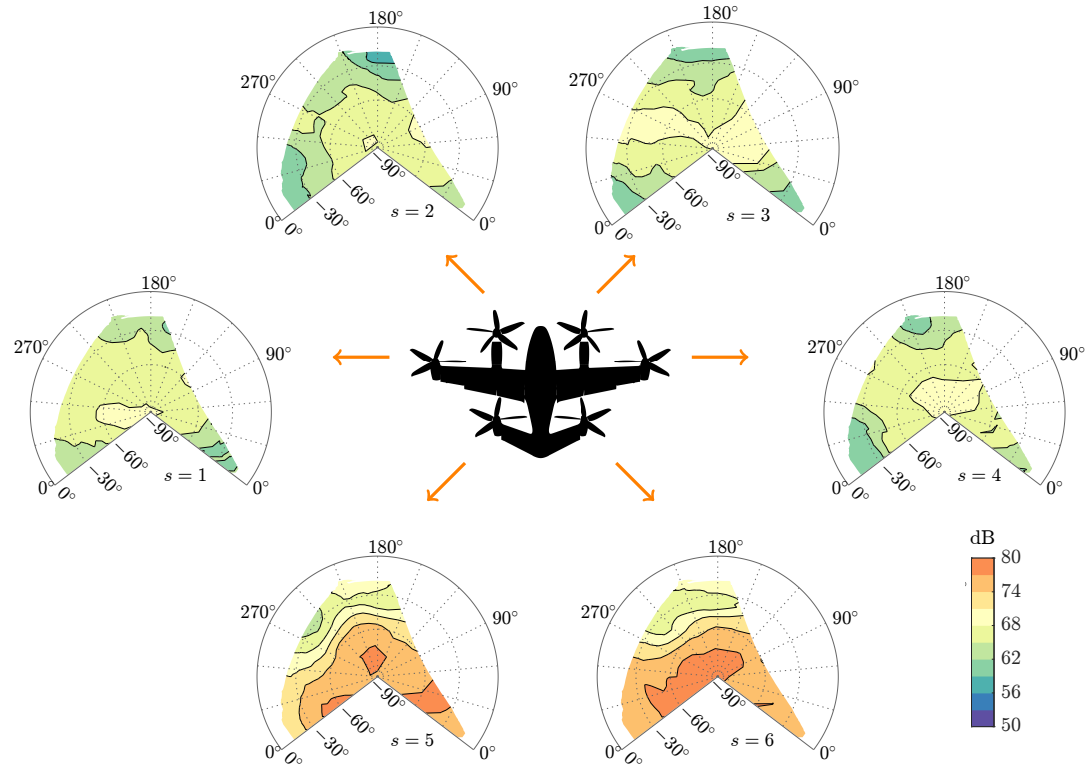


**(a) Experiment + Vold-Kalman Filter**

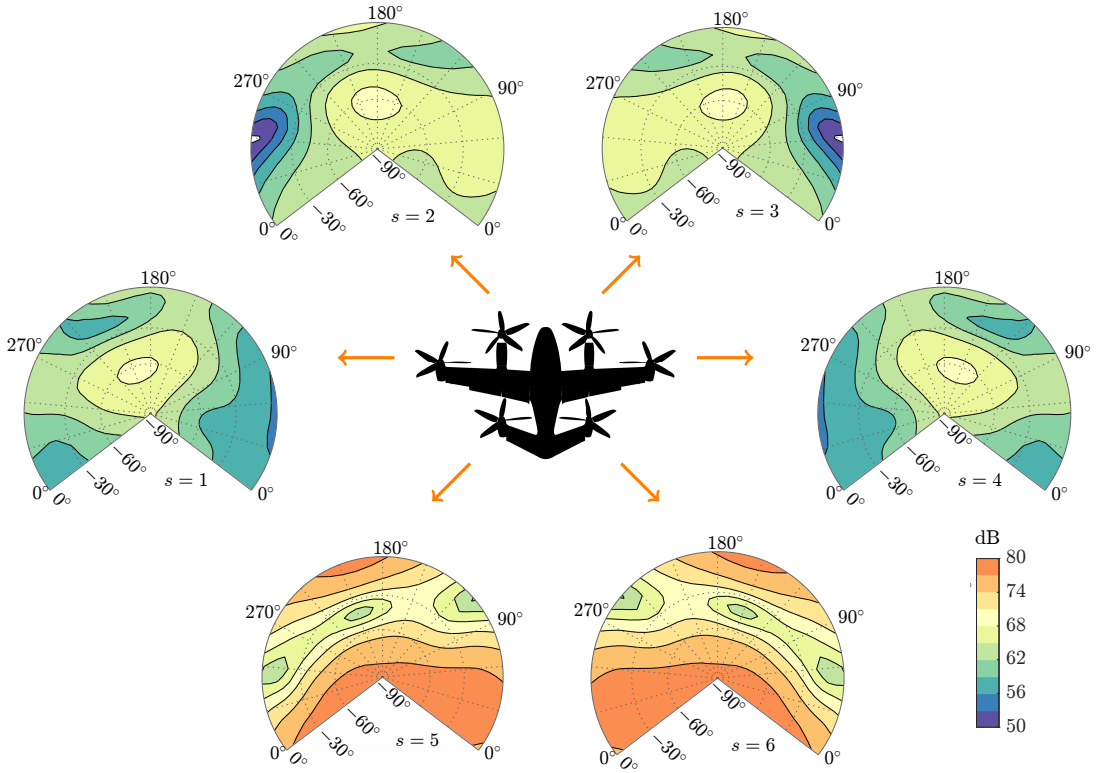


**(b) OVERFLOW/PSU-WOPWOP**

**Fig. 12 Individual propeller integrated (shaft order 2 to 25) 100 ft acoustic hemispheres.**

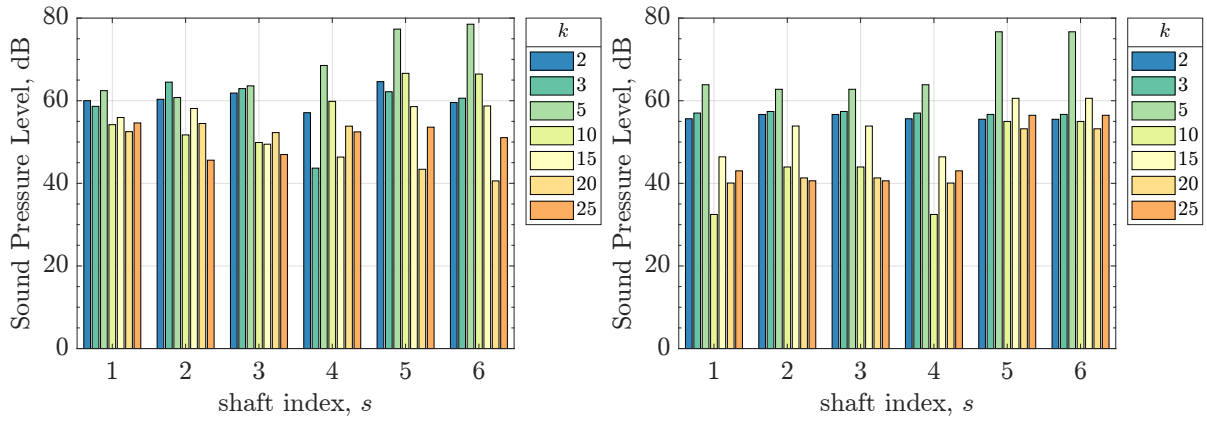


**(a) Experiment** **(b) CFD**

**Fig. 13 Comparison between V-K-filtered and predicted shaft sound pressure levels per order for the Joby aircraft in steady level flight at 60 knots at a microphone near -90 deg elevation. The levels were adjusted to distance of 100 ft assuming spherical spreading.**

The individual propeller sound level hemispheres, summed over shaft orders 2 to 25 ($k = 2, 3, 5, 10, 15, 20, 25$), are plotted in Fig. 12. There is good agreement in both directivity and magnitude between the CFD-predicted and V-K-filtered results. The rotation direction and placement of the propellers with respect to the airframe have a big impact on the directivity. The predicted results for the propeller pairs are symmetric due to the assumptions of the CFD model. Although the V-K-filtered results are not symmetric, there is some agreement in the hotspots, which are generally near lower elevation angles. Both methods are able to capture the larger levels on the tail propellers that are caused by the ingestion of the wake from the front propellers. There is also reasonable agreement in the directivity of the tail propellers, which is generally below and behind the aircraft.

The sound pressure level per order and per shaft index was computed for a single observer near -90 deg elevation and compared to experimental data. The results are plotted in Fig. 13. The CFD predicts a dominant BPF across all propellers, with a level that is at least 5 dB greater than the other shaft orders. The experiment reflects a similar trend except for the inboard propellers ($s = 2 - 3$), where the lower three orders are relatively similar in magnitude ($k = 2, 3, 5$). Looking at both the V-K filter and CFD results, the influence of the tail propellers is further highlighted here. Interestingly, the CFD results in higher levels at $k = 20$ and $k = 25$ for the tail propellers compared to the others, but the measurement does not. Inspecting the aircraft symmetry for this microphone, the mean difference in levels between propellers in a pair across all orders is 6.10 dB for the wingtip propellers, 2.85 dB for the inboard propellers, and 1.93 dB for the tail propellers. This is significantly different from that of hover, where the mean difference was 2.66 dB. This could indicate that, if the separation method is working correctly, the wingtip propellers could potentially experience greater acoustic variability at this flight condition. The tail propellers, whose main noise source is from the aerodynamic interaction, exhibit the lowest variability. On the other hand, the CFD result has no difference due to the symmetry assumption. It should be noted that this flight condition is not typical of the nominal mission profile as the aircraft is typically in transition at this airspeed. Application of the V-K filter to a greater variety of flight conditions could yield further insight into the noise sources and aid in determining quieter trim states.

## VI. Conclusions and Future Work

The Vold-Kalman (V-K) filter was applied to the Joby Aviation aircraft in hover and steady level flight at 60 knots to identify the acoustic contributions of individual propellers. High-fidelity simulations of both conditions using NASA OVERFLOW and PSU-WOPWOP were conducted for validation. In hover, the CFD predicted the overall sound pressure level very well, with predictions lying within the experimental

range for all but one microphone. Comparisons of V-K-filtered results with CFD predictions for the BPF SPL yielded reasonable agreement for both conditions in terms of both magnitude and directivity. However, the inboard propeller directivities were flipped and the differences were attributed to assumptions in the model. Nonetheless, the mean model difference between V-K-filtered and CFD results across all microphones, propellers, and shaft orders was 1.75 dB, which indicates very good agreement. For the case of steady level flight at 60 knots, the CFD predicted the overall sound pressure level reasonably well. Both the V-K filter and the CFD were able to capture the increased levels from the tail propellers due to the aerodynamic interactions. The asymmetry in the shaft order levels between propeller pairs reveals that the wingtip propellers experience the largest acoustic variability in this flight condition. The control law implemented during the flight test campaign in 2021 is, however, not reflective of that of the production aircraft. For both flight conditions, the method should be applied to different runs at the same condition during the flight test to investigate the repeatability of the results. Overall, the agreement between the V-K filter and the CFD prediction yields confidence in the methods and illuminates the noise sources, which could help aircraft designers. It should be noted that the focus in this paper was on low frequency content, which could potentially be less important for human perception. It is still uncertain as to which sound quality metrics will be most representative in community noise assessments.

Ongoing research focuses on applying the V-K filter to other flight conditions to examine the feasibility of the approach. Other flight conditions may have more constant and more similar rotation rates, as well as other noise sources. All of these effects could impact the utility of the method. The CFD showed discrepancies in the inboard propeller directivity in hover and in the symmetry across propeller pairs for both conditions. Future work should explore the effects of rotor phasing, atmospheric turbulence, airframe acoustic shielding, and unsteadiness in the CFD simulations. These are all considerations that will affect results when conducting flight tests in an outdoor environment and will have an impact on operations. These phenomena did not have a large impact on the comparison for these flight conditions, but may be more important for conditions with higher variability such as takeoff and landing. High-fidelity CFD simulations typically take days on hundreds of cores to obtain acoustic data for a single trim state at a single airspeed. The V-K filter could be an excellent alternative for noise source separation and identification for eVTOL developers once a flight-capable vehicle is available.

## References


[1] Stoll, A., and Bevirt, J., "Development of eVTOL Aircraft for Urban Air Mobility At Joby Aviation," *Vertical Flight Society 78th Annual Forum*, Fort Worth, TX, May, 2022. https://doi.org/10.4050/F-0078-2022-17528.

[2] Bain, J., Goetchius, G., and Josephson, D., "Flyover Noise Comparison Between Joby Aircraft and Similar Aircraft," *Vertical Flight Society 78th Annual Forum*, Fort Worth, TX, May, 2022. https://doi.org/10.4050/F-0078-2022-17437.

[3] Stephens, D. B., and Vold, H., "Order Tracking Signal Processing for Open Rotor Acoustics," *Journal of Sound and Vibration*, Vol. 333, No. 16, August, 2014, pp. 3818–3830. https://doi.org/10.1016/j.jsv.2014.04.005.

[4] Vold, H., and Leuridan, J., "High Resolution Order Tracking at Extreme Slew Rates Using Kalman Tracking Filters," *Noise and Vibration Conference and Exposition*, Traverse City, MI, May, 1993. https://doi.org/10.4271/931288.

[5] Rachaprolu, J. S., and Greenwood, E., "Helicopter Noise Source Separation Using an Order Tracking Filter," *Journal of the American Helicopter Society*, Vol. 69, January, 2024, pp. 1–9. https://doi.org/10.4050/JAHS.69.012006.

[6] Thai, A., Bain, J., Mikić, G. V., and Stoll, A., "Flyover Noise Computations of the Joby Aviation Aircraft," *Vertical Flight Society 79th Annual Forum*, West Palm Beach, FL, May, 2023. https://doi.org/10.4050/F-0079-2023-17959.

[7] Roget, B., Lim, J., Sitaraman, J., Bain, J., Escobar, D., Thai, A., and Jude, D., "Multi-Fidelity Investigation of Aerodynamics and Acoustics of the Joby Aviation Aircraft using CREATE$^{TM}$ AV Helios," *Vertical Flight Society 80th Annual Forum*, Montréal, Canada, May, 2024.

[8] Pascioni, K. A., Watts, M. E., Houston, M. L., Lind, A. H., Stephenson, J. H., and Bain, J. J., "Acoustic Flight Test of the Joby Aviation Advanced Air Mobility Prototype Vehicle," *28th AIAA/CEAS Aeroacoustics Conference*, Southampton, UK, June, 2022. https://doi.org/10.2514/6.2022-3036.

[9] Tůma, J., "Setting the Passband Width in the Vold-Kalman Order Tracking Filter," *Twelfth International Congress on Sound and Vibration*, Lisbon, Portugal, July, 2005.

[10] Tůma, J., "Algorithms for the Vold-Kalman multiorder tracking filter," *Proceedings of the 14th International Carpathian Control Conference*, Rytro, Poland, May, 2013. https://doi.org/10.1109/CarpathianCC.2013.6560575.

[11] Pascioni, K. A., Thai, A. D., and Bain, J. J., "Propeller Source Noise Separation from Flight Test Measurements of the Joby Aviation Aircraft," *30th AIAA/CEAS Aeroacoustics Conference*, Rome, Italy, June, 2024.

[12] Nichols, R. H., Tramel, R. W., and Buning, P. G., "Solver and Turbulence Model Upgrades to OVERFLOW 2 for Unsteady and High-Speed Applications," *24th Applied Aerodynamics Conference*, San Francisco, CA, June, 2006. https://doi.org/10.2514/6.2006-2824.

[13] Tramel, R. W., Nichols, R. H., and Buning, P. G., "Addition of Improved Shock-Capturing Schemes to OVERFLOW 2.1," *19th AIAA Computational Fluid Dynamics Conference*, San Antonio, TX, June, 2009. https://doi.org/10.2514/6.2009-3988.

[14] Derlaga, J. M., Jackson, C. W., and Buning, P. G., "Recent Progress in OVERFLOW Convergence Improvements," *AIAA Scitech 2020 Forum*, Orlando, FL, January, 2020. https://doi.org/10.2514/6.2020-1045.

[15] Spalart, P., and Allmaras, S., "A One-Equation Turbulence Model for Aerodynamic Flows," *Proceedings of the 30th Aerospace Sciences Meeting and Exhibit*, Reno, Nevada, January, 1992. https://doi.org/10.2514/6.1992-439.

[16] Spalart, P. R., Deck, S., Shur, M. L., Squires, K. D., Strelets, M. K., and Travin, A., "A New Version of Detached-eddy Simulation, Resistant to Ambiguous Grid Densities," *Theoretical and Computational Fluid Dynamics*, Vol. 20, No. 3, May, 2006, pp. 181–195. https://doi.org/10.1007/s00162-006-0015-0.

[17] Coder, J., Pulliam, T. H., and Jensen, J. C., "Contributions to HiLiftPW-3 Using Structured, Overset Grid Methods," *Proceedings of the 2018 AIAA Aerospace Sciences Meeting*, Kissimmee, FL, January, 2018. https://doi.org/10.2514/6.2018-1039.

[18] Toro, E. F., Spruce, M., and Speares, W., "Restoration of the Contact Surface in the HLL-Riemann Solver," *Shock Waves*, Vol. 4, No. 1, July, 1994, pp. 25–34. https://doi.org/10.1007/BF01414629.

[19] Brentner, K. S., and Farassat, F., "Modeling Aerodynamically Generated Sound of Helicopter Rotors," *Progress in Aerospace Sciences*, Vol. 39, No. 2-3, February-April, 2003, pp. 83–120. https://doi.org/10.1016/S0376-0421(02)00068-4.

[20] Thai, A., and Bain, J., "Modeling Approach and Departure Noise of the Joby Aviation Aircraft," *Vertical Flight Society 80th Annual Forum*, Montréal, Canada, May, 2024.